Applied Surface Science 447 (2018) 269–278

Contents lists available at ScienceDirect

Applied Surface Science

journal homepage: www.elsevier.com/locate/apsusc

Full Length Article

Potential applications of three-dimensional structure of silk fibroin/poly (ester-urethane) urea nanofibrous scaffold in heart valve tissue engineering

Juan Du [a], Tonghe Zhu [b], Haiyan Yu [a], Jingjing Zhu [b], Changbing Sun [a], Jincheng Wang [a], Sihao Chen [a,*], Jihu Wang [a,*], Xuran Guo [b]

[a] College of Chemistry and Chemical Engineering, Shanghai University of Engineering Science, Shanghai 201620, People's Republic of China
[b] State Key Laboratory for Modification of Chemical Fibers and Polymer Materials, College of Chemistry, Chemical Engineering and Biotechnology, Donghua University, Shanghai 201620, People's Republic of China

ARTICLE INFO

Article history:
Received 7 January 2018
Revised 5 March 2018
Accepted 9 March 2018
Available online 10 March 2018

Keywords:
Silk fibroin
Poly(ester-urethane) urea elastomer
Nanofiber
Electrospinning
Heart valve tissue engineering

ABSTRACT

Tissue engineering heart valves (TEHV) are thought to have many advantages in low immunogenicity, good histocompatibility, excellent mechanical properties. In this paper, we reported the fabrication and characterization of a novel composite nanofibrous scaffold consisting of silk fibroin (SF) and poly (ester-urethane) urea (LDI-PEUU) by using electrospinning. Chemical and physical properties of scaffolds were evaluated using scanning electron microscopy, attenuated total reflectance Fourier transform infrared, X-ray diffraction, contact angle measurement, thermogravimetric analysis, biodegradation test and tensile strength analysis. We determined that the composite scaffolds supported the growth of human umbilical vein endothelial cell (HUVEC). The results of cell proliferation and cell morphology indicate that SF/LDI-PEUU nanofibers promoted cell viability, which supporting the application in tissue engineering. All results clarified that SF/LDI-PEUU (40:60) nanofibrous scaffolds meet the required specifications for tissue engineering and could be used as a promising construct for heart valve tissue engineering.

1. Introduction

In spite of the major advances with regard to regenerative medicine approaches [1], valvular heart disease remains to be a significant global health problem. Several methods such as pharmacological therapy and heart transplantation are applied for regeneration of heart valve [2,3]. However, xenogenic grafts are associated with the risk of immunogenic reactions and the availability of homografts is limited. Therefore, biodegradable natural materials have been studied for the fabrication of autologous tissue engineered heart valves (TEHVs) [4]. In heart valve tissue engineering, development of the composite scaffold is critical as it is the main tensile load bearer and excellent biocompatibility.

As a natural protein, silk fibroin (SF) is one of the earliest animal protein used in the past. SF derived from silkworm plays a crucial role in biomedical applications and tissue engineering [5]. Silkworm is mainly composed of silk fibroin coated with sericin, and their content is over 95%. Besides, there is a small amount of carbohydrates and other impurities in silkworm. SF structure is mainly composed of glycine (46%), alanine (29%), serine (18%) and other 18 kinds of amino acids [6]. SF consists of a light (L) chain polypeptide and a heavy (H) chain polypeptide linked together via a single disulfide bond at the C-terminus of H-chain, forming a H–L complex [7]. With the development of research on the structure and properties of silk [8–10], the application of SF in biomaterials has been paid more and more attention. SF is considered to be one of the biological materials with the most applicative prospect, due to the unique properties of excellent biocompatibility [11], control of excellent mechanical properties [12], biodegradability [13,14], hemocompatibility, cytocompatibility and its interactions with cells. In the meaning time, the well-oriented β-sheet structure of SF gives it good mechanical properties such as good flexibility, tensile strength and moisture permeability. However, for some mechanically demanding organizations, the mechanical properties of electrospun fibrous scaffolds are not sufficient to meet the requirements of the organization [15]. After the treatment of methanol and ethanol, the fracture strength of SF scaffold can be improved, but the fracture resistance of the fiber scaffold is reduced and the brittleness characteristic cannot meet the requirements of the organization [16]. Therefore, taking advantage of synthetic polymers which with good mechanical properties,

* Corresponding authors.
E-mail addresses: chensh@sues.edu.cn (S. Chen), wangjihu@163.com (J. Wang).

https://doi.org/10.1016/j.apsusc.2018.03.077
0169-4332/

electrospinning to prepare blended fiber scaffolds, to obtain biocompatibility and mechanical properties of both tissue engineering scaffold.

Polyurethane (PU) is one of the most popular synthetic polymers which applied in tissue engineering field [17]. Poly (ester-urethane) urea segmented block copolymers are used in a variety of biomedical applications, most prominently as blood sacs in ventricular assist devices and total hearts in the blood vessels [18–21]. These materials are solution-processable elastomers that exhibit good mechanical properties [22], versatile processability, tunable properties, while simultaneously exhibiting good in vivo biocompatibility [23]. With the mixture of SF and LDI-PEUU, the blended stent can not only maintain excellent biological properties, but also improve the mechanical properties of SF.

Till now, various methods have been utilized to process SF into particles, fibers, films, and gels for a variety of applications. For example, phase separation, self-assembly [24], gas foaming, etc. Electrospinning has been recognized as one of the most simple and versatile methods to produce nanofibers which diameters in the nanoscale range of 50–1000 nm [25,26]. Generally, electrospun nanofibers with different fiber diameters exhibit a wide range of surface properties (hydrophilicity, hydrophobicity, high specific surface area, porosity) and superior mechanical properties (stress, tensile strength, Young's modulus, elongation at break) compared to the other forms of materials [27]. The electrospinning method allows SF and LDI-PEUU to be combined effectively. Electrospun fiber membrane with high specific surface area, high porosity also meet the requirements of tissue engineering scaffold. On the one hand, electrospun nanofibers provide high surface to volume ratio, suitable surface topography for cell adhesion and attachment and high porosity. On the other hand, electrospun nanofibers exhibit superior mechanical properties with desired anti - deformation ability, resistance to strain deformation and compression deformation [28]. Now electrospinning is widely used for the development of tissue engineering scaffolds that closely mimic the size and scale of the natural extracellular matrix (ECM) [29,30], due to its unique properties, including high specific surface area and excellent biocompatibility. For example, Salvador Aznar-Cervantes et al. studied the silk fibroin scaffolds via electrospinning for applications in biomedicine [31]. Fang J et al. studied the modification of PEUU with heparin and endothelium-inducing peptide aiming for vascular reconstruction [32]. It is presumed that SF/LDI-PEUU composites had good biocompatibility, mechanical property, and potential clinical application for heart valve tissue engineering [33–35]. Thus, it is obvious that composite nanofibers have more promising prospects.

To accomplish this task, the material interface should mimic the biophysical and the biochemical properties of heart valve to meet the needs of heart valve tissue engineering. In this study, SF was prepared from silkworm, composite nanofibers of SF/LDI-PEUU has been fabricated by electrospinning. Then, the mechanical properties, chemical structure, surface wettability, thermal properties, degradation properties, and biocompatibility of this composite nanofibers scaffolds have been tested.

2. Materials and methods

2.1. Materials

Silk fibroin (SF), which derived from silkworm. L-lysine diisocyanate poly(ester-urethane) urea elastomer (LDI-PEUU), was synthesized by Shanghai University of Engineering Science (Shanghai, China). 1, 1, 1, 3, 3, 3-hexafluoro-2-propanol (HFIP) were purchased from Titan Technology Co., Ltd (Shanghai, China). Phosphate buffered saline (PBS) and 3-(4, 5-Dimethylthiazol-2-yl)-2, 5-diphenyltetrazoliumbromide (MTT) were obtained from Sigma Co., Ltd (USA). Dulbecco's modified Eagle's medium (DMEM), fetal bovine serum (FBS), antibiotic–antimycotic and trypsin were purchased from Shanghai Yuanxiang Medical Equipment Co., Ltd (Shanghai, China).

2.2. Silk fibroin extraction

Silkworms were chopped into 3 or 4 pieces, boiled in 0.5% (w/v) Na_2CO_3 for 30 min and repeated 3 times to remove the glue-like sericin proteins. Then, the raw SF was rinsed thoroughly with ultrapure water, extruded with water and dried overnight at 60 °C. The extracted SF was dissolved in 9.3 M LiBr for 4 h at 60 °C, to generate a 20 wt% solution that was dialyzed against distilled water for 3 days (Snakeskin Dialysis Tubing 14 KDa MWCO, Thermo Scientific). The SF solution after dialysis was lyophilized for 24 h to obtain the regenerated SF sponges [36]. The components of silkworms were shown in Table 1.

2.3. Electrospinning of nanofibers

The nanofibers were prepared via electrospinning process (Fig. 1). Briefly, SF and LDI-PEUU with different mass ratios (SF/LDI-PEUU = 100:0, 80:20, 60:40, 50:50, 40:60, 20:80, 0:100) were dissolved in HFIP with the different concentration (Table 2), the polymer solution was poured into 5.0 mL plastic syringes with blunt-ended needles and via traditional electrospinning equipment, which consisting of a syringe pump, a high voltage supplier and a collector to make into a randomly oriented electrospun scaffolds. Syringes were placed on syringe pumps and propelled at a rate of 1.0 mL/h. The high voltage power supplies with the voltage of 10 kV were applied across the needles and ground collectors and the receive distance is 15 cm. All of the electrospinning processes were carried out at room temperature and 50% ± 2% relative humidity. Finally, the samples were placed in a vacuum oven for 4 days. The parameters of the seven groups of nanofibrous scaffolds were presented in Table 2.

2.4. Nanofibrous scaffolds characterization

The surface structure and the morphology of the SF/LDI-PEUU nanofibers was observed with scanning electron microscopy (Phenom, Phenom XL, Netherlands). The electrospun nanofibrous scaffolds were sputter coated with gold to impart conductivity at an accelerating voltage of 10 kV. The average fiber diameter was determined from 100 random measurements on a typical SEM image using Image analysis software (Image-J, National Institutes of Health, USA). In addition, surface topography of SF/LDI-PEUU nanofibrous scaffolds was inspected with an atomic force microscope (AFM) (Multimode & Dimension3100, Varian, USA).

The chemical bonds and functional groups present in the nanofibrous scaffolds were analyzed by using a attenuated total reflectance Fourier transform infrared spectrometer (ATR-FTIR, Thermo Nicolet, Waltham, MA, USA) in the range of 4000–400 cm^{-1}.

Wide-angle X-ray diffraction (WAXRD) for the nanofibers was obtained with a D/Max-2550PC diffractometer (Rigaku Co., Tokyo, Japan). WAXRD data was collected over a 2 range of 10–80°.

Wettability of the nanofibrous scaffolds were examined by contact angle measurement equipment (OCA40, Data-physics, Germany). The angle of contact made by the water droplet with the nanofibrous scaffolds surface revealed the degree of hydrophilicity of the samples. 5 parts of the same sample were analyzed and get the average data.

The mechanical properties of the nanofibrous scaffolds were studied by a universal test frame machine (H5K-S, Hounsfield,

Table 1
The components of silkworms.

Component	SF	Sericin	Carbohydrates	Wax	Ash	Pigment
Content (%)	70–80	20–30	1.2–1.6	0.4–0.8	0.7	0.2

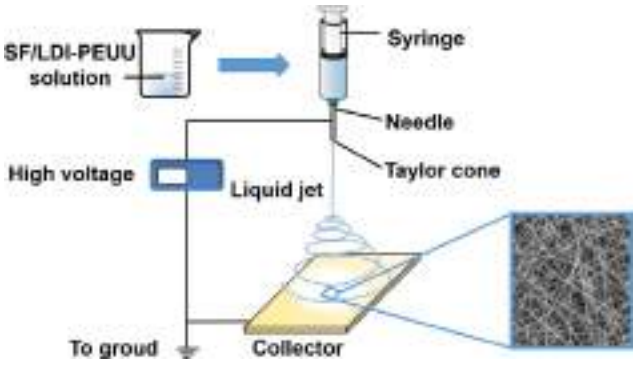

Fig. 1. Schematic illustration of the experimental procedures for fabricating the nanofibrous scaffold.

UK). Specimens (50 mm × 10 mm, n = 3) were tested with the ambient temperature and were recorded with a crosshead speed of 50 mm/min. The sample of SF nanofibrous scaffolds were tested with a crosshead speed of 1 mm/min due to the poor toughness of SF.

Thermogravimetric analysis was characterized by using SDT Q600 V20.9 Build 20 instrument (TA, American). Samples (5–10 mg) under 10 °C/min rate from 25 °C to 900 °C with a Nitrogen which rate was 100.0 mL/min.

The hydrolytic degradation of electrospun nanofibrous scaffolds were studied in vitro during 4 weeks. The nanofibrous scaffolds were cut into slices (5 mg) and placed in vials containing 10 mL of phosphate buffer solution (PBS, pH = 7.4). Moreover, all the samples should be sealed up and put on a shaker in 37 °C to mimic the natural environmental conditions and taken out at 1, 2, 4 weeks to measure their properties.

2.5. Hemolysis assays

Hemolysis assays was performed with fresh New Zealand white rabbit blood. In brief, fresh white rabbit blood was collected which containing 3.8% sodium citrate injection (the ratio of anticoagulant to blood is 1:9, v/v). Then, healthy red blood cells (HRBC) were obtained by centrifugation at 1200 r/min for 5 min, and washed the precipitates with physiologic saline buffer for 3 times to remove the serum. The HRBCs were diluted with physiologic saline buffer before hemolysis assay. The sterilized SF/LDI-PEUU nanofibrous scaffolds (50 mg) were added into centrifugal tube with physiologic saline buffer (10 mL) at 37 °C for 30 min before 0.2 mL diluted HRBCs were added. In comparison, the diluted HRBCs (0.2 mL) were also mixed with 10 mL distilled water (as a positive control), and mixed with 10 mL physiologic saline buffer (as a negative control). Afterwards, all the sample tubes were incubated at 37 °C for 1 h and taken away carefully. The HRBC suspensions were centrifuged at 1200 r/min for 5 min to get clear supernatant fluids. The absorbance of supernatant was measured by Lambda 25 UV–Vis spectrophotometer (Perkin Elmer, USA) at 545 nm. The hemolysis ratio (HR) was defined as follow:

$$HR = \frac{SA - NA}{PA - NA} \times 100\%$$

where SA, PA, NA were the absorbency of the sample, the positive control (distill water) and negative control (physiologic saline), respectively. Mean and standard deviation of the triplicate centrifugal tubes for each sample were calculated.

2.6. Cell culture and viability assay

HUVECs were grown in Dulbecco's modified Eagle's medium (DMEM) with 10% fatal bovine serum (FBS), 1% antibiotic–antimycotic under the atmosphere of 5% CO_2 and 37 °C. The culture media was changed every two days. All samples were placed into 24-well plate and fixed by stainless steel rings. Then, samples were sterilized with 70% ethanol immersion for 12 h and washed 3 times by using phosphate buffer solution (PBS), and washed once again with culture medium. After that, the HUVECs were seeded on the membrane with a density of 1.0×10^4 cells per well of 24-well plate.

3-[4, 5-dimethylthiazol-2-yl]-2, 5-diphenyltetrazolium-bromide (MTT) assay [37] and cells SEM were performed to evaluate the viability and morphology of the proliferated HUVECs which grow on different nanofibrous scaffolds, three sample for every material. The time points of test were set as 1, 4, and 7 days [38,39]. At each point, the culture plates were taken out of the incubator and removed the culture medium, then the samples were washed with PBS. MTT solution (1 mg/mL in test medium) was added (40 μL/dish) to the well, and the scaffolds were incubated at 37 °C for 4 h. Four hours later, the precipitates were dissolved in DMSO and the optical density (OD) of the extracted medium was tested by microplate reader at the wavelength of 492 nm.

2.7. Statistical analysis

Origin8.0 (Origin Lab Inc., USA) was applied for statistical analysis. All results are represented as the mean ± standard deviation (SD). The data were analyzed by one-way ANOVA, followed by Tukey's test for the evaluation of specific differences and the data were indicated significant at $p < 0.05$.

Table 2
The process parameters of nanofibrous scaffolds.

Sample	Solute	SF/LDI-PEUU ratio (w/w)	Solvent	Concentration
1	SF	100:0	HFIP	20%
2	SF/LDI-PEUU	80:20	HFIP	18%
3	SF/LDI-PEUU	60:40	HFIP	16%
4	SF/LDI-PEUU	50:50	HFIP	15%
5	SF/LDI-PEUU	40:60	HFIP	14%
6	SF/LDI-PEUU	20:80	HFIP	13%
7	LDI-PEUU	0:100	HFIP	12%

3. Results and discussion

3.1. Morphology of the nanofibrous scaffolds

The surface morphology and topography of the electrospun nanofibrous scaffolds of the different materials were acquired at different magnifications by SEM and AFM (Fig. 2). The microscopic images obtained by SEM showed a framework constituted by randomly-oriented fibers [7,12]. In all cases the surface of the nanofibers was smooth and the surface of these nanofibers display a porous three-dimensional structure [40]. Besides, AFM showed that the surface of SF/LDI-PEUU nanofibers were homogenous and randomly-oriented and also display a porous three-dimensional structure. However, the results suggest that there was some difference in the morphology of different nanofibers, the surface morphology of nanofibers were becoming less and less obvious with the increase of LDI-PEUU ratio. The diameter of SF was 289 ± 76 nm and LDI-PEUU was 465 ± 165 nm. LDI-PEUU was better in electrospinning, but LDI-PEUU had good elasticity and fiber characteristics were not obvious. The picture of the fiber diameter distributed that there was a uniform distribution for all nanofibrous scaffolds and the mean fiber diameters increased with the increase percentage of LDI-PEUU. The diameter of SF/LDI-PEUU (80:20) decreased compare to SF nanofibers, this phenomenon can be explained by the conductivity of the mixed solution. SF is a typical amphoteric polymer electrolyte, consisting of highly repeating amino acids such as glycine and alanine and a large side chain containing a charged amino acid. When LDI-PEUU was added to the spinning solution, the charge density of the solution increases, and the stretching effect of the static electricity on the jet was enhanced, which resulting in the generation of fine fibers.

To visualize the surface wettability of the seven nanofibrous scaffolds, the dynamic water contact angle was measured. The contact angle results showed that the hydrophilicity of scaffolds significantly decreased by increasing the ratio of LDI-PEUU within the composite, which is likely due to multiple hydrophobic functional groups in chemical structure of LDI-PEUU. The increase in contact angle was not conducive to the rapid wetting of the material on the

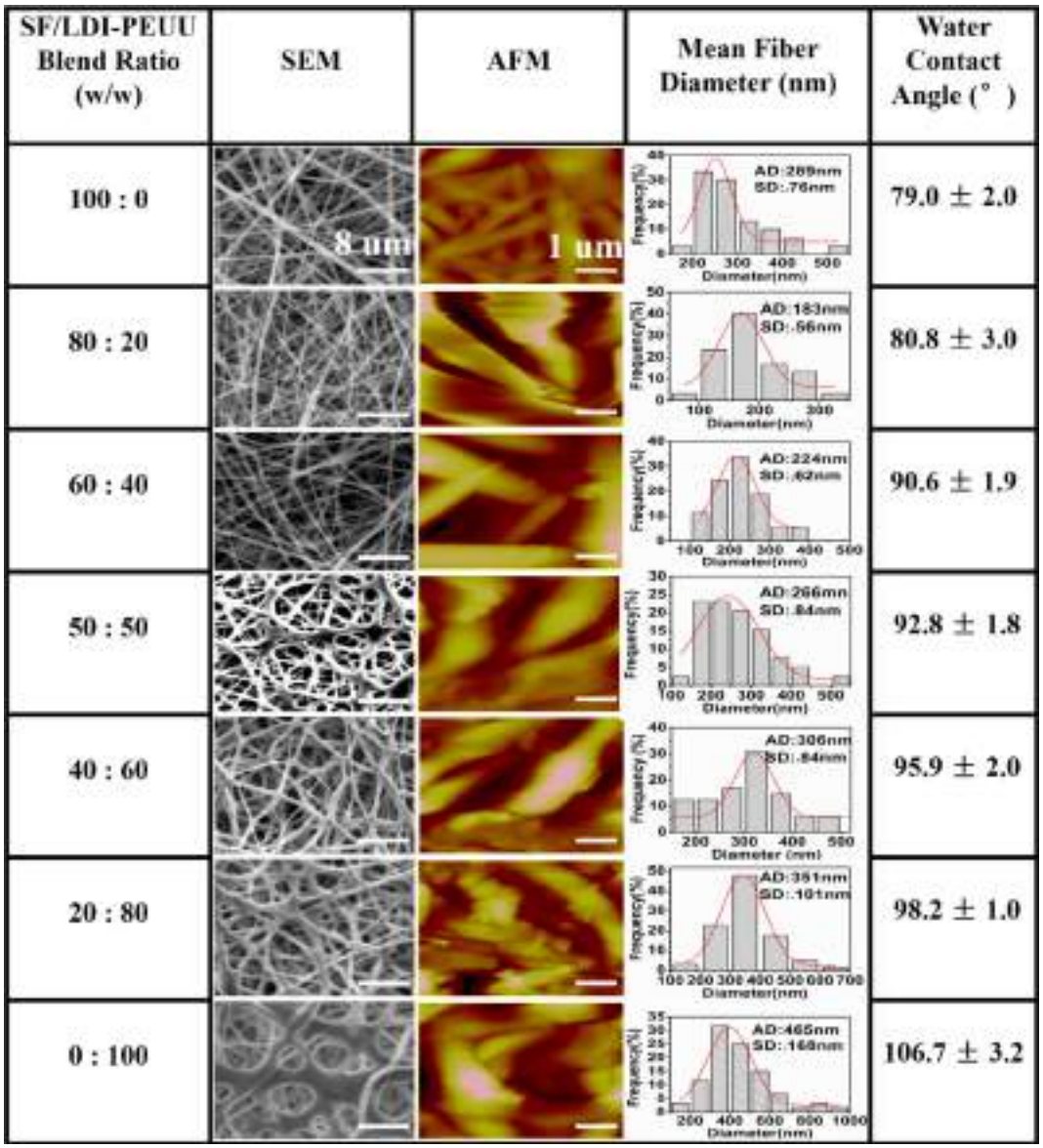

Fig. 2. SEM images, AFM images, nanofiber diameter distribution and water contact angle of SF/LDI-PEUU nanofibrous scaffolds with different ratios. The scale bar of SEM is 8 μm and the scale of AFM is 1 μm.

surface and the rapid cell adhesion [46]. However, if extend the infiltration time, when the scaffold was completely wetted by the liquid, the larger surface area of the hydrophobic material surface would provide more sites for cell adhesion. Looking at the above factors, the surface wettability of the most nanofibrous scaffolds tended to be hydrophilic and might be contribute to cell proliferation.

3.2. Chemical structure of SF/LDI-PEUU nanofibrous scaffolds

The molecular structure of SF and LDI-PEUU was showed in Fig. 3(c) and (d), respectively. The presence of the infrared spectrum showed the characteristic peaks of SF and LDI-PEUU (Fig. 3). In SF, the strong peak at 1643.05 cm^{-1} (amide I) represented the stretching vibration of C═O, and the peak at 1533.18 cm^{-1} (amide II) represented the presence of N—H. All those peaks suggested that the presence structure of SF. In addition, the peak at 3283.76 cm^{-1} showed the presence of O—H. These main peaks indicated that amide I, II and III were the important functional groups of SF. As can be seen in Fig. 3(a), all the peaks in the FTIR spectrum of SF are also observed in the FTIR spectra of nanofibers containing SF and LDI-PEUU. With the increase of LDI-PEUU ratio, which shown in Fig. 3(a), the intensities of the peaks at 1643.05 cm^{-1}, 1533.18 cm^{-1} represent the structure of SF gradually decreased by increasing the ratio of LDI-PEUU. FTIR spectra of LDI-PEUU demonstrated ester, urethane, and urea groups, as shown by the pronounced carbonyl peak of the ester at 1733 cm^{-1} and its shoulder peak at lower wavelength, which is attributable to hydrogen-bond association of the urethane and urea groups [19]. The intensities of the peaks at 3000–2700 cm^{-1} and 1700–1000 cm^{-1} represent the structure of LDI-PEUU. It means, the characteristic peaks of SF and LDI-PEUU are appear in the nanofibers, with the increase of LDI-PEUU content, the characteristic peak intensity of SF decreased, and the peak intensity of LDI-PEUU increased. The same absorption peaks of SF/LDI-PEUU nanodibrous scaffolds indicate that SF and LDI-PEUU blends will not change their molecular structure.

The WAXRD results of nanofibrous scaffolds were depicted in Fig. 3(b), from which could be concluded that the diffraction peak of samples were appeared at 2θ equaled to 21°, 30°, separately. SF nanofibers had relatively weak diffraction peak near 20° and 30°, which corresponding to Silk II and silk I crystal structures of silk fibroin, respectively. SF appears a weak diffraction peak at 20.7°, indicating that SF is mainly amorphous structure and there is a small amount of silk I type crystal structure. These crystalline structures may be caused by the shearing action during the electrospinning process and the rearrangement of the silk fibroin molecules during the curing process. A sharp peak that may represent the crystalline structure of the soft segment in SF/LDI-PEUU materials. The nanofibers with different contents of LDI-PEUU have a diffraction peak at 21°, and the diffraction peak becomes sharper with the increases of LDI-PEUU content, indicating that the addition of LDI-PEUU increases the crystallinity of SF/LDI-PEUU nanofibers. This θ phenomenon may due to the appearance of new bonds in LDI-PEUU.

3.3. Mechanical properties of nanofibers

The representative tensile stress–strain curves and mechanical properties of SF/LDI-PEUU nanofibrous scaffolds are tested respec-

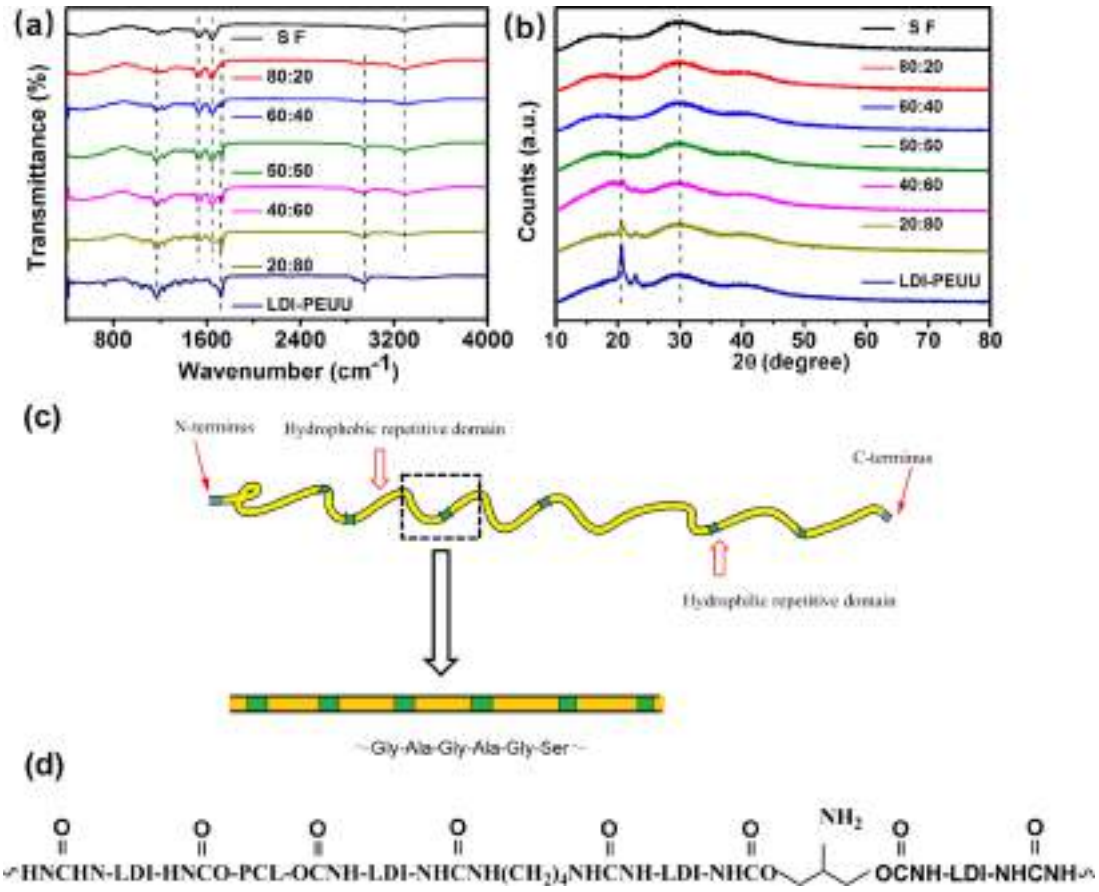

Fig. 3. (a) ATR-FTIR spectra of SF/LDI-PEUU nanofibrous scaffolds with different ratios; (b) X-ray diffraction of SF/LDI-PEUU nanofibrous scaffolds; (c) the molecular structure of SF; (d) the molecular backbone of LDI-PEUU based polymers.

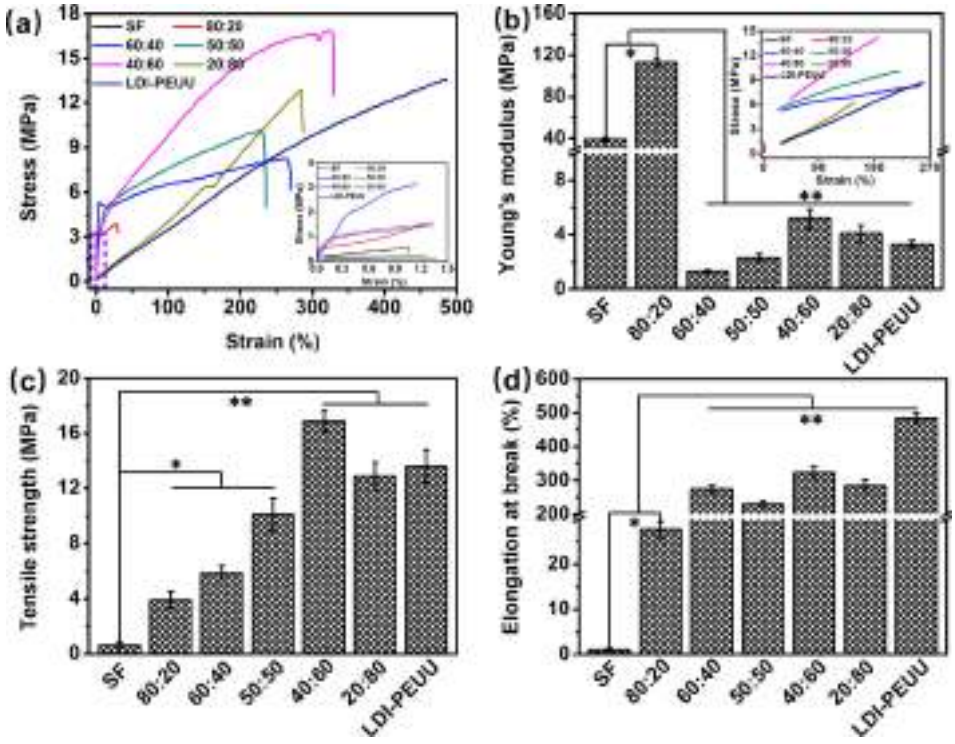

Fig. 4. Mechanical of SF/LDI-PEUU nanofibrous scaffolds with different ratios: (a) representative stress–strain curves, inset shows the magnification stress–strain curves; (b) Young's modulus, inset shows the magnification Young's modulus curves; (c) Tensile strength; (d) Elongation at break. *Indicates a significant difference from others ($p < 0.05$); **indicates a significant difference from others ($p < 0.01$).

tively, and the data are shown in Fig. 4 and Table 3. The Young's modulus (Fig. 4(b)), tensile strength (Fig. 4(c)), elongation at break (Fig. 4(d)) of all samples were summarized as well. SF nanofibrous scaffold is too brittle and the practical application of SF is limited. Therefore, it is necessary to add LDI-PEUU to improve its mechanical properties and promote its practical application [14,20]. Compared with SF nanofiber, LDI-PEUU nanofibers has high strength and toughness, which can improve the brittleness of electrospinning nanofibers and enhance toughening. The results suggest that the fracture stress of SF nanofibrous scaffolds is 0.56 MPa and LDI-PEUU nanofibrous scaffolds is 13.50 MPa. The fracture strain of SF nanofibrous scaffolds is 1.05% and LDI-PEUU nanofibrous scaffolds is 485.95%. With the increase of LDI-PEUU content, the fracture stress and fracture strain of the blended nanofibrous scaffolds increased, especially the fracture strain was improved obviously. The fracture stress of SF/LDI-PEUU (40:60) nanofibrous scaffolds is better than other nanofibrous scaffolds. The elongation at break of SF/LDI-PEUU (80:20) nanofibrous scaffolds increased significantly from 1.05% of SF to 30.96%. The results suggested that the mechanical properties of nanofibers are improve with the increase of LDI-PEUU ratio. It means that the addition of LDI-PEUU improves the mechanical properties of SF. The increase in the elongation at break of SF/LDI-PEUU nanofibrous scaffolds compared to SF nanofibrous scaffolds may due to the interaction between the amino groups.

In practical applications, different biological tissue on the mechanical performance of alternative stents are also different, such as heart valve scaffold requires a good fatigue resistance. Therefore, the mechanical properties of the blended scaffold can be adjusted by adjusting the material blending ratio to suit the needs of different tissue engineering.

Table 3
Tensile properties of SF/LDI-PEUU nanofibrous scaffolds with different ratio (data are representatives of independent experiments and all data are given as mean ± SD, n = 3).

SF/LDI-PEUU Blend Ratio (w/w)	Young's modulus (MPa)	Tensile strength (MPa)	Elongation at break (%)
100:0	38.6 ± 2.1	0.6 ± 0.2	1.1 ± 0.3
80:20	112.9 ± 3.5	3.9 ± 0.6	27.7 ± 1.8
60:40	1.3 ± 0.1	5.9 ± 0.5	274.9 ± 10.6
50:50	2.3 ± 0.3	10.1 ± 1.2	230.1 ± 9.9
40:60	5.2 ± 0.7	16.9 ± 0.8	323.4 ± 17.9
20:80	4.1 ± 0.6	12.9 ± 1.0	284.5 ± 17.1
0:100	3.3 ± 0.3	13.6 ± 1.2	485.0 ± 15.8

3.4. Thermal decomposition properties of SF/LDI-PEUU nanofibers

Thermogravimetric analysis is the most important way of studying the thermal stability of compounds (Fig. 5). The rate of nanofibrous scaffolds descending are relatively slow before 100 °C, it may due to the vaporization of water in nanofibrous scaffolds. The results suggest that the weight decreased rapidly from approximately 50 °C to 400 °C, which is due to the thermal decomposition of the material. At 200 °C, the polymer itself shrinks to release small molecules and the polymer chain breaks to release small molecules, then the polymer begins to decompose. It can be indicated that the starting temperature of the thermal degradation of the seven nanofibrous scaffolds is about 200 °C to 250 °C. Meanwhile, when the weight dropped to 50%, the thermal temperature is about 300 °C. From the initial temperature curve of the thermal decomposition of the material in the Fig. 5. The results suggest that the loss of the thermal decomposition weight of SF/LDI-PEUU materials decrease with the increase of the LDI-PEUU ratio at 200 °C. This trend may due to the interaction between active groups in LDI-PEUU, such as ester group and amino, tightly entanglement of molecular chains are formed to slow down the rate of thermal decomposition.

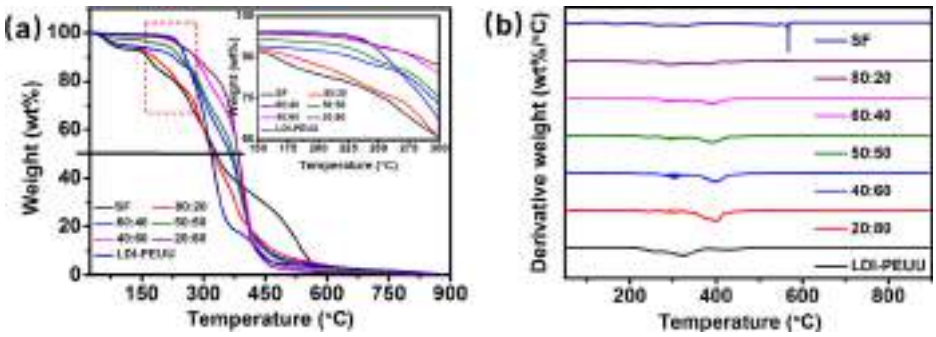

Fig. 5. Thermal degradation of SF/LDI-PEUU nanofibrous scaffolds with different ratios as measured through TGA. (a) TG curves and (b) DTG curves.

Fig. 5(b) shows the peak decomposition temperature of nanofibrous scaffolds. It suggested that the DTG curves reveal the decomposition temperature which the maximum weight loss rate is reached. From Fig. 5(b), it can be observed that the peak decomposition temperature of SF nanofibrous scaffold appears about 570 °C, and LDI-PEUU nanofibrous scaffold appears about 325 °C. The chain structure of LDI-PEUU decreased the temperature of thermal decomposition [20]. In the electrospun blends, the two melting peaks of SF and LDI-PEUU merge and appear as a broad peak with a center point between the two melting points of SF and PEUU. This indicates that the elongational flow during spinning favors the more stable crystal formation. In addition, a peak of cold crystallization in SF is due to the movement of the chains into a more organized crystalline structure. Therefore, the results proved that the blend fibers are more stable than the pure SF fibers.

3.5. Biodegradability in vitro

The biodegradability of the material is an important property of the tissue engineering scaffold [16,18]. The degradation rate of nanofibrous scaffold needs to match the rate of tissue growth. If the scaffold degradation is too quickly, the new tissue will lose its function and fail to repair the target tissue. If the scaffold degradation is too slowly, the scaffold will hinder the formation of the new tissue.

The weight loss of nanofibers during degradation is shown in Fig. 6(a). The results demonstrated that the degradation of SF was the fastest, which may due to SF can dissolved in water and dissolved in the PBS solution quickly. In order to improve the degradation of SF, and promote its application in tissue engineering, we blend SF with LDI-PEUU. It can be indicated from Fig. 6 (a) that the addition of LDI-PEUU slowed down the degradation rate of SF significantly. Furthermore, the weight loss decreased with the increase of PEUU content in SF/LDI-PEUU nanofibrous scaffolds.

During the degradation process [41,42], the weight loss is caused by some of the soluble oligomeric compounds on the surface of polymer. The compounds are dispersed and dissolved in the degradation medium produced by the hydrolysis cracking of the polymer chains. LDI-PEUU is a hydrophobic polymer, the degradation rate of penetrating into the scaffold is slow and the degradation rate is limited. The picture shows that the weight of LDI-PEUU almost constant during the degradation process. Therefore, the degradation rate of composites can be regulated by changing the blend ratio of SF and LDI-PEUU. The results suggest that the degradation rate of SF/LDI-PEUU nanofibrous scaffolds are become more and more slowly with the increase of LDI-PEUU.

SEM image of SF/LDI-PEUU nanofibrous scaffolds during the degradation process for 1, 2 and 4 weeks are shown in Fig. 6(b). SF/LDI-PEUU nanofibrous scaffolds was partly dissolved since the first week. After degradation for 4 weeks, most of the nanofibrous scaffolds appeared to varying degrees of degradation, but the fiber structure of scaffolds was well remained. This attribute would be conduced to the silk I structure (random coil) of SF converted to silk II (β-sheet) in PBS solution, which molecules are arranged closely and not easy to break. Compare with LDI-PEUU nanofibrous scaffold, the fibers on the SF/LDI-PEUU nanofibrous scaffolds are broken or melted, but no obvious morphological change was found in SF/LDI-PEUU nanofibrous scaffolds till 4 weeks except for SF/LDI-PEUU nanofibrous scaffolds (60:40). This may cause by the ratio of LDI-PEUU in composite nanofibrous scaffolds. With the increase of LDI-PEUU, the degree of degradation gradually weakened. As the degradation time increases, the degree of degradation of the scaffold is gradually increased, and the fiber fracture and swelling are gradually obvious. The results indicated that the typical morphological change of SF/LDI-PEUU nanofibrous nanofibers during degradation was fiber breaking. It was believed that the polymer chains of SF and LDI-PEUU in the crystalline region were rigid and immobilized, which caused the breakage of fibers when there was a "weak" point along the fiber axis during degradation [42]. In addition, the random coil of pure SF is a crystalline structure which is easy to dissolve in water and cause the dissolve in PBS solution.

3.6. Hemocompatibility of SF/LDI-PEUU nanofibrous scaffolds

The hemolytic activity of implant materials is one of the decisive factors to evaluate blood compatibility. As a xenogenous graft, the physical and chemical agents on its surface could damage erythrocytes, which leading to the release of hemoglobin. For potential heart valve prosthesis materials, the degree of erythrolysis of SF/LDI-PEUU nanofibrous saffolds is used to evaluate the destructive potential that implants present to erythrocytes.

The hemolysis test results of SF/LDI-PEUU nanofibrous scaffolds are shown in Fig. 7. It is suggested that all the hemolysis rate (HR) of SF/LDI-PEUU nanofibrous scaffolds are far less than 5% (value reported in the literature). The results indicated that blood compatibility of SF/LDI-PEUU is good enough to be cardiac valve prosthesis. In addition, the HR of SF and LDI-PEUU nanofibrous scaffold is about 1.83% and 1.36%, which both of them have good blood compatibility and can be used as valve materials. Previously, it had already been demonstrated that the hemocompatibility of SF/LDI-PEUU nanofibrous scaffolds is excellently suited for tissue engineering application, especially for cardiac valve. Furthermore, compare with SF/LDI-PEUU nanofibrous scaffolds, the HR of SF/LDI-PEUU nanofibrous scaffold (40:60) is lower than others. It is concluded that the hemocompatibility of SF/LDI-PEUU nanofibrous scaffold (40:60) is better than other scaffolds.

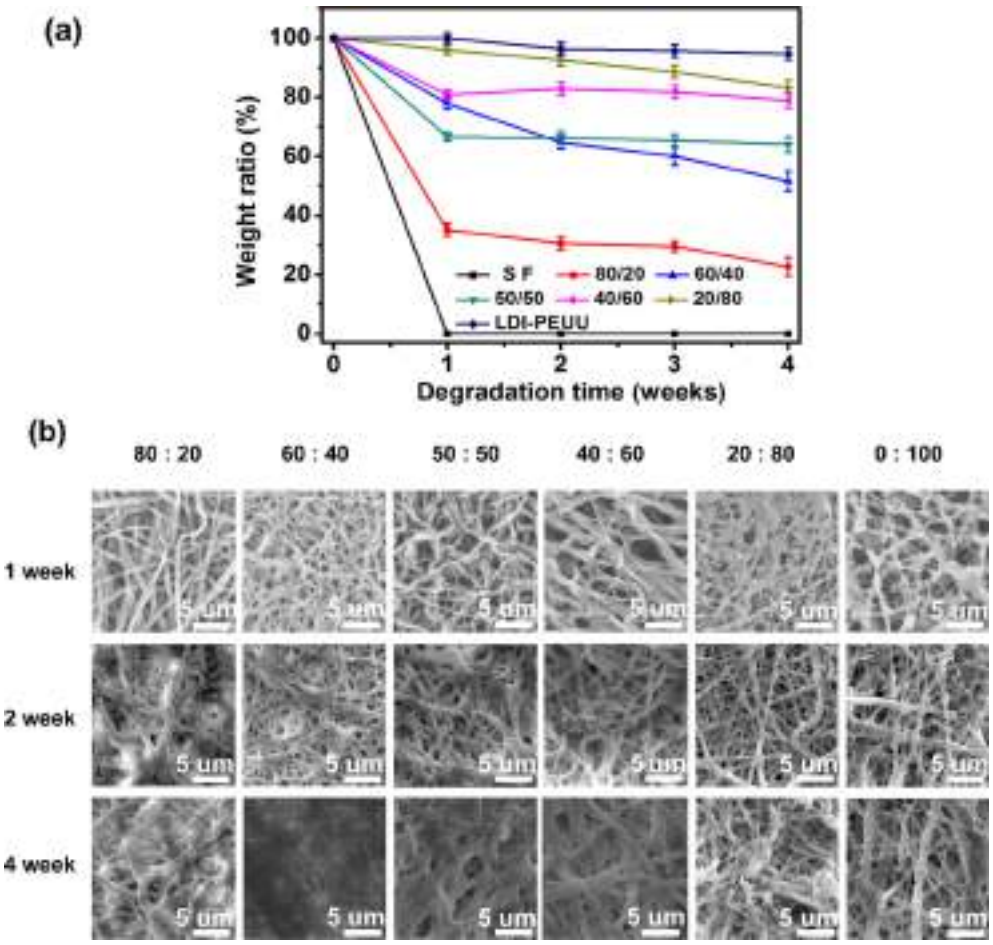

Fig. 6. (a) Weight loss of SF/LDI-PEUU nanofibrous scaffolds during degradation. (b) Scanning electron micrographs of SF/LDI-PEUU nanofibrous scaffolds with different ratio after biodegradation for different periods in PBS; bar = 5 μm.

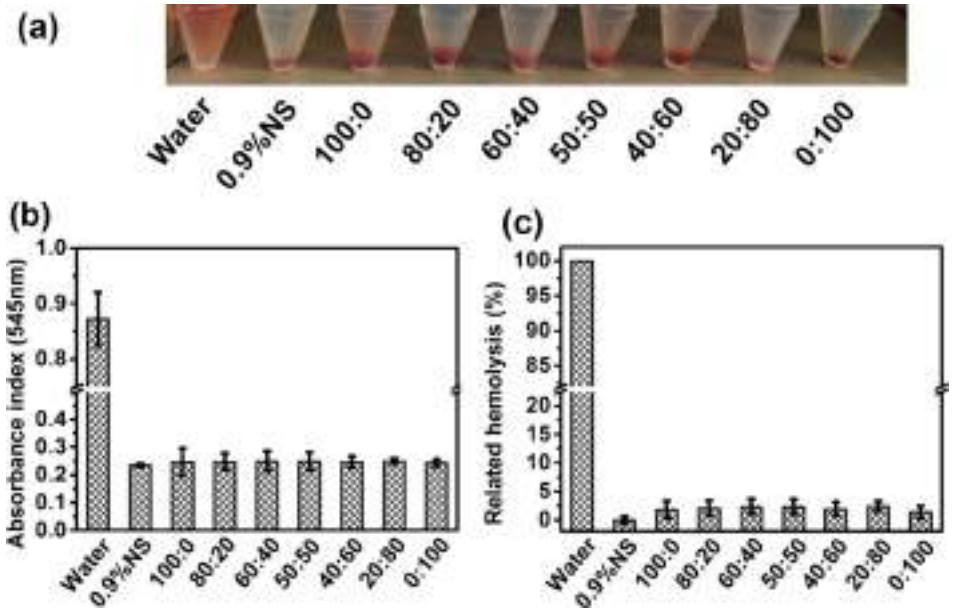

Fig. 7. Hemolysis assay of SF/LDI-PEUU nanofibrous scaffolds in contact with blood in vitro (n = 3). The photograph shows the hemolytic condition after centrifugation (a); absorbance index at 545 nm (b); hemolysis rate (c). Water (+) and 0.9% physiologic saline (−) was used as positive and negative control, respectively.

3.7. In vitro cell culture of the nanofibrous scaffolds

For further tissue engineering applications, it is important to ensure the biocompatibility of the developed nanofibrous scaffolds. Fig. 8(A) illustrates the effects of the scaffolds on the viability of HUVECs in comparison to cover slips. In previous studies, SF containing RGD was proved to be an excellent biomaterial for tissue engineering application [47]. The HUVECs morphology on SF/LDI-PEUU nanofibrous scaffolds are shown in Fig. 8(B). The in vitro cytocompatibility study showed that the nanocomposite films fabricated in this study were not toxic to HUVECs.

It is noted that cell response to the biomaterials is affected by both the mean fiber diameter of materials and mechanical properties. Distribution of LDI-PEUU in SF matrix not only changed the mean fiber diameter of the scaffolds, but also increased the mechanical properties of the scaffolds. The result indicated that there was no statistical difference between the scaffolds during the incubation periods at day 1. After 4 days, compared with the cover slips, the cells can proliferate better on the composite nanofibrous scaffolds, suggesting that the nanofibrous scaffolds can provide more adhesion points and the addition of LDI-PEUU improve the mechanicl properties, which favor cell adhesion and proliferation. It is concluded that HUVECs cultured on SF are rounded and scattered, which may due to the collapse of silk fibroin nanofiber and the cells cannot continue to adhere to grow. Further, SF/LDI-PEUU (0:100) show poor cell proliferation properties compared to the other samples. It may due to the mean fiber diameter of LDI-PEUU was significantly higher than composite scaffolds and the strong hydrophobicity of LDI-PEUU. These properties of LDI-PEUU lead it cannot simulate the extracellular matrix (ECM) [30], and the cell adhesion effect is not as good as the composite scaffolds. By contrast, the morphology of the cells on SF/LDI-PEUU nanofibrous scaffolds (80:20, 40:60) is spindle-shaped and spreads well on the surface of the SF/LDI-PEUU nanofibrous scaffolds. Overall, the above results indicate that the prepared SF/LDI-PEUU composite scaffolds have greater potential for use as heart valve in comparison to SF scaffold and LDI-PEUU scaffold. This indicates that SF/LDI-PEUU nanofibrous scaffolds has promising potential for application in tissue engineering [27,43–45].

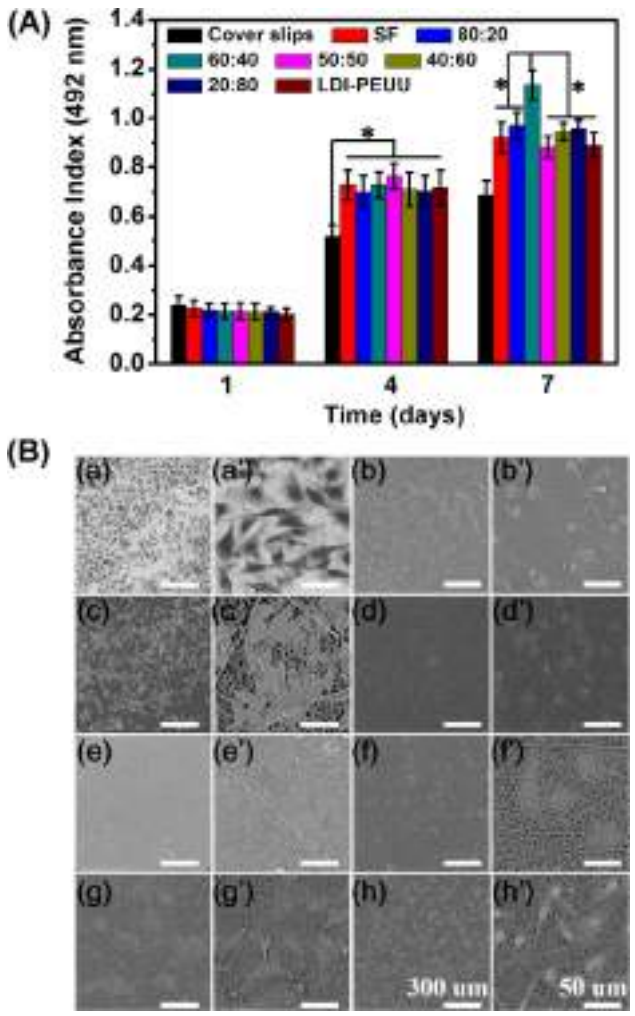

Fig. 8. (A) Cell proliferation results of cytocompatibility of SF/LDI-PEUU nanofibrous scaffolds at 1, 4, and 7 days via MTT. *Indicates a significant difference from others ($p < 0.05$). (B) SEM micrographs of HUVECs on the cover slips and SF/LDI-PEUU nanofibrous scaffolds with different ratis. Cover slips (a and a′); SF/LDI-PEUU 100:0 (b and b′); SF/LDI-PEUU 80:20 (c and c′); SF/LDI-PEUU 60:40 (d and d′); SF/LDI-PEUU 50:50 (e and e′); SF/LDI-PEUU 40:60 (f and f′); SF/LDI-PEUU 20:80 (g and g′); SF/LDI-PEUU 0:100 (h and h′). The scale bar of ((a)–(h)) is 300 mm and the scale bar of ((a′)–(h′)) is 50 mm.

4. Conclusion

In the present study, a series of SF/LDI-PEUU nanofibrous scaffolds were fabricated by electrospinning. The nanofibrous scaffolds were evaluated via mechanical and thermal analysis, and degradation process. The degradation rate and tensile property of the composite material can be adjusted by changing the ratio of SF and LDI-PEUU. The cells viability evaluations further highlighted the biocompatibility of the samples when in contact with HUVECs for 1, 4 and 7 days. Our results indicated that, although incorporation of LDI-PEUU led to slightly decrease the hydrophilic of SF scaffolds, it was in favor of enhancing the mechanical properties and cells proliferation, as the sample with LDI-PEUU content exhibited more suitable tensile properties and cells viability compared with pure SF and LDI-PEUU. These results suggest that the as-prepared SF/LDI-PEUU (60:40) nanofibrous scaffold may be a promising application in heart valve tissue engineering.

Notes

The authors declare no competing financial interest.

Acknowledgements

The authors sincerely appreciate the support of “Capacity Building Project of Some Local Colleges and Universities in Shanghai (Grant No. 17030501200)”, “National Natural Science Foundation (Grant No. 81501595)”, “Youth Foundation of Zhongshan Hospital (Grant No. 2015ZSQN09)”, “Talent Training Program Foundation for the Excellent Youth Supported by Zhongshan Hospital (Grant No. 2017ZSYQ24)”, and “Innovation Fund of Zhongshan Hospital (Grant No. 2017ZSCX05)”.

References

[1] A. Rising, Controlled assembly: a prerequisite for the use of recombinant spider silk in regenerative medicine, Acta Biomater. 10 (2014) 1627–1631.
[2] Alessandra Di Franco, Giulia Cantini, Alessia Tani, Sodium-dependent glucose transporters (SGLT) in human ischemic heart: A new potential pharmacological target, Int. J. Cardiol. 243 (2017) 86–90.
[3] R.K. Iyer, L.L.Y. Chiu, L.A. Reis, M. Radisic, Engineered cardiac tissues, Curr. Opin. Biotechnol. 22 (2011) 706–714.
[4] J. Usprech, D.A. Romero, C.H. Amon, C.A. Simmons, Combinatorial screening of 3D biomaterial properties that promote myofibrogenesis for mesenchymal stromal cell-based heart valve tissue engineering, Acta Biomater. 58 (2017) 34–43.
[5] W.H. Zhou, Z.J. Jia, P. Xiong, J.L. Yan, Y.Y. Li, M. Li, Y. Cheng, Y.F. Zhenie, Bioinspired and biomimetic AgNPs/gentamicin-embedded silk fibroin coatings for robust antibacterial and osteogenetic applications, ACS Appl. Mater. Inter. 9 (2017) 25830–25846.

[6] J. Brown, C.L. Lu, J. Coburn, D.L. Kaplan, Impact of silk biomaterial structure on proteolysis, Acta Biomater. 11 (2015) 212–221.
[7] L.D. Koh, Y. Cheng, C.P. Teng, Y.W. Khin, X.J. Loh, S.Y. Tee, M. Low, E.Y. Ye, H.D. Yu, Y.W. Zhang, Structures, mechanical properties and applications of silk fibroin materials, Prog. Polym. Sci. 46 (2015) 86–110.
[8] J. Guan, D. Porter, F. Vollrath, Thermally induced changes in dynamic mechanical properties of native silks, Biomacromolecules 14 (2013) 930–937.
[9] Z. Li, Z.K. Zheng, Y.H. Yang, G.Q. Fang, J.R. Yao, Z.Z. Shao, X. Chen, Robust protein hydrogels from silkworm silk, ACS Sustain. Chem. Eng. 4 (2016) 1500–1506.
[10] X. Hu, K. Shmelev, L. Sun, E.-S. Gil, S.-H. Park, P. Cebe, D.L. Kaplan, Regulation of silk material structure by temperature-controlled water vapor annealing, Biomacromolecules 12 (2011) 1686–1696.
[11] Y.F. Feng, X.F. Li, M.Z. Li, D.Z. Ye, Q. Zhang, R.C. You, W.L. Xu, Facile preparation of biocompatible silk fibroin/cellulose nanocomposite films with high mechanical performance, ACS Sustain. Chem. Eng. 5 (2017) 6227–6236.
[12] F. Teulé, Y.G. Miao, B.H. Sohn, Y.S. Kim, J.J. Hull, M.J. Fraser, R.V. Lewis, D.L. Jarvis, Silkworms transformed with chimeric silkworm/spider silk genes spin composite silk fibers with improved mechanical properties, Proc. Natl. Acad. Sci. U.S.A. 109 (2012) 923–928.
[13] A. Teimouri, M. Azadi, R. Emadi, J. Lari, A.N. Chermahini, Preparation, characterization, degradation and biocompatibility of different silk fibroin based composite scaffolds prepared by freeze-drying method for tissue engineering application, Polym. Degrad. Stabil. 121 (2015) 18–29.
[14] F.M. Miroiu, N. Stefan, A.I. Visan, C. Nita, C.R. Luculescu, O. Rasoga, M. Socol, I. Zgura, R. Cristescu, D. Craciun, Composite biodegradable biopolymer coatings of silk fibroin-poly(3-hydroxybutyric-acid-co-3-hydroxyvaleric-acid) for biomedical applications, Appl. Surf. Sci. 355 (2015) 1123–1131.
[15] F.F. Zhou, X.Z. Zhang, D.D. Cai, J. Li, Q. Mu, W. Zhang, S.A. Zhu, Y.Z. Jiang, W.L. Shen, S.F. Zhang, Silk fibroin-chondroitin sulfate scaffold with immuno-inhibition property for articular cartilage repair, Acta Biomater. 63 (2017) 64–75.
[16] S.S. Silva, N.M. Oliveira, M.B. Oliveira, D.P.S. da Costa, D. Naskar, J.F. Mano, S.C. Kundu, R.L. Reis, Fabrication and characterization of Eri silk fibers-based sponges for biomedical application, Acta Biomater. 32 (2016) 178–189.
[17] I. Adipurnama, M.C. Yang, T. Ciach, B. Butruk-Raszeja, Surface modification and endothelialization of polyurethane for vascular tissue engineering applications: a review, Biomater. Sci. 5 (2017) 22–37.
[18] J. Fang, S.H. Ye, V. Shankarraman, Y.X. Huang, X.M. Mo, W.R. Wagner, Biodegradable poly(ester urethane) urea elastomers with variable amino content for subsequent functionalization with phosphorylcholine, Acta Biomater. 10 (2014) 4639–4649.
[19] K. Yu, T.H. Zhu, Y. Wu, X.X. Zhou, X.C. Yang, J. Wang, J. Fang, H. El-Hamshary, S. S. Al-Deyab, X.M. Mo, Incorporation of amoxicillin-loaded organic montmorillonite into poly(ester-urethane) urea nanofibers as a functional tissue engineering scaffold, Coll. Surf. B-Biointer. 151 (2017) 314–323.
[20] T.H. Zhu, K. Yu, M.A. Bhutto, X.R. Guo, W. Shen, J. Wang, W.M. Chen, H. El-Hamshary, S.S. Al-Deyab, X.M. Mo, Synthesis of RGD-peptide modified poly (ester-urethane) urea electrospun nanofibers as a potential application for vascular tissue engineering, Chem. Eng. J. 315 (2017) 177–190.
[21] J. Fang, S.H. Ye, J. Wang, T. Zhao, X.M. Mo, W.R. Wagner, Thiol click modification of cyclic disulfide containing biodegradable polyurethane urea elastomers, Biomacromolecules 16 (2015) 1622–1633.
[22] D.W. Park, S.-H. Ye, H.B. Jiang, D. Dutta, K. Nonaka, W.R. Wagner, K. Kim, In vivo monitoring of structural and mechanical changes of tissue scaffolds by multi-modality imaging, Biomaterials 35 (2014) 7851–7859.
[23] P.A. Nair, P. Ramesh, Electrospun biodegradable calcium containing poly(ester-urethane) urea: Synthesis, fabrication, in vitro degradation, and biocompatibility evaluation, J. Biomed. Mater. Res. A 101 (2013) 1876–1887.
[24] J. Bauer, T. Scheibel, Dimerization of the conserved N-terminal domain of a spider silk protein controls the self-assembly of the repetitive core domain, Biomacrmolecules 18 (2017) 2521–2528.
[25] S. Jana, A. Cooper, F. Ohuchi, M.Q. Zhang, Uniaxially aligned nanofibrous cylinders by electrospinning, ACS Appl. Mater. & Inter. 4 (2012) 4817–4824.
[26] M. Kitsara, O. Agbulut, D. Kontziampasis, Y. Chen, P. Menasche, Fibers for hearts: A critical review on electrospinning for cardiac tissue engineering, Acta Biomater. 48 (2017) 20–40.
[27] P. Karuppuswamy, J.R. Venugopal, B. Navaneethan, A.L. Laiva, S. Sridhar, S. Ramakrishna, Functionalized hybrid nanofibers to mimic native ECM for tissue engineering applications, Appl. Surf. Sci. 322 (2014) 162–168.
[28] G.X. Zhao, X.H. Zhang, T.J. Lu, F. Xu, Recent Advances in Electrospun nanofibrous scaffolds for cardiac tissue engineering, Adv. Funct. Mater. 25 (2015) 5726–5738.
[29] J.M. Aamodt, D.W. Grainger, Extracellular matrix-based biomaterial scaffolds and the host response, Biomaterials 86 (2016) 68–82.
[30] B. Trappmann, J.E. Gautrot, J.T. Connelly, D.G.T. Strange, Y. Li, M.L. Oyen, M.A.C. Stuart, H. Boehm, B.J. Li, V. Vogel, Extracellular-matrix tethering regulates stem-cell fate, Nat. Mater. 11 (2012) 642–649.
[31] S. Aznar-Cervantes, M.I. Roca, J.G. Martinez, L. Meseguer-Olmo, J.L. Cenis, J.M. Moraleda, T.F. Otero, Fabrication of conductive electrospun silk fibroin scaffolds by coating with polypyrrole for biomedical applications, Bioelectrochemistry 85 (2012) 36–43.
[32] J. Fang, J.L. Zhang, J. Du, Y.J. Pan, J. Shi, Y.X. Peng, W.M. Chen, L. Yuan, S.H. Ye, W.R. Wagner, Orthogonally functionalizable polyurethane with subsequent modification with heparin and endothelium-inducing peptide aiming for vascular reconstruction, ACS Appl. Mater. Inter. 8 (2016) 14442–14452.
[33] A.G. Guex, A. Frobert, J. Valentin, G. Fortunato, D. Hegemann, S. Cook, T.P. Carrel, H.T. Tevaearai, M.N. Giraud, Plasma-functionalized electrospun matrix for biograft development and cardiac function stabilization, Acta Biomater. 10 (2014) 2996–3006.
[34] C. Patra, S. Talukdar, T. Novoyatleva, S.R. Velagala, C. Mühlfeld, B. Kundu, S.C. Kundu, F.B. Engel, Silk protein fibroin from antheraea mylitta, for cardiac tissue engineering, Biomaterials 33 (2012) 2673–2680.
[35] B. Kundu, R. Rajkhowa, S.C. Kundu, X.G. Wang, Silk fibroin biomaterials for tissue regenerations, Adv. Drug. Deliver. Rev. 65 (2013) 457–470.
[36] D.N. Rockwood, R.C. Preda, T. Yücel, X. Wang, M.L. Lovett, D.L. Kaplan, Materials fabrication from Bombyx mori silk fibroin, Nat. Protoc. 6 (2011) 1612–1631.
[37] N.E. Davis, L.N. Beenken-Rothkopf, A. Mirsoian, N. Kojic, D.L. Kaplan, A.E. Barron, M.J. Fontaine, Enhanced function of pancreatic islets coencapsulated with ECM proteins and mesenchymal stromal cells in a silk hydrogel, Biomaterials 33 (2012) 6691–6697.
[38] L.C. Su, H. Xu, R.T. Tran, Y.T. Tsai, L.P. Tang, S. Banerjee, J. Yang, K.T. Nguyen, In situ re-endothelialization via multifunctional nanoscaffolds, ACS Nano 8 (2014) 10826–10836.
[39] C.W. McCarthy, D.C. Ahrens, D. Joda, T.E. Curtis, P.K. Bowen, R.J. Guillory, S.Q. Liu, F. Zhao, M.C. Frost, J. Goldman, Fabrication and short-term in vivo performance of a natural elastic lamina-polymerichybrid vascular graft, ACS Appl. Mater. Inter. 7 (2015) 16202–16212.
[40] M.B. Applegate, J. Coburn, B.P. Partlow, J.E. Moreau, J.P. Mondia, B. Marelli, D.L. Kaplan, F.G. Omenetto, Laser-based three-dimensional multiscale micropatterning of biocompatible hydrogels for customized tissue engineering scaffolds, Proc. Natl. Acad. Sci. U.S.A. 112 (2015) 12052–12057.
[41] N.R. Raia, B.P. Partlow, M. McGill, E.P. Kimmerling, C.E. Ghezzi, D.L. Kaplan, Enzymatically crosslinked silk-hyaluronic acid hydrogels, Biomaterials 131 (2017) 58–67.
[42] R.C. You, Y.M. Xu, Y. Liu, X.F. Li, M.Z. Li, Comparison of the in vitro and in vivo degradations of silk fibroin scaffolds from mulberry and nonmulberry silkworms, Biomed. Mater. 10 (2015) 1.
[43] H.G.S. Ayaz, A. Perets, H. Ayaz, K.D. Gilroy, M. Govindaraj, D. Brookstein, P.I. Lelkes, Textile-templated electrospun anisotropic scaffolds for regenerative cardiac tissue engineering, Biomaterials 35 (2014) 8540–8552.
[44] E.S. Jamadi, L. Ghasemi-Mobarakeh, M. Morshed, M. Sadeghi, M.P. Prabhakaran, S. Ramakrishna, Synthesis of polyester urethane urea and fabrication of elastomeric nanofibrous scaffolds for myocardial regeneration, Mater. Sci. Eng. C-Mater. 63 (2016) 106–116.
[45] S.I. Voicu, R.M. Condruz, V. Mitran, A. Cimpean, F. Miculescu, C. Andronescu, M. Miculescu, V.K. Thakur, Sericin Covalent immobilization onto cellulose acetate membrane for biomedical applications, ACS Sustain. Chem. Eng. 4 (2016) 1765–1774.
[46] A.C.B. Allen, E. Barone, C.O. Crosby, L.J. Suggs, J. Zoldan, Electrospun poly(N-isopropyl acrylamide)/poly(caprolactone) fibers for the generation of anisotropic cell sheets, Biomater. Sci. 5 (2017) 1661–1669.
[47] S. Behera, D. Naskar, S. Sapru, P. Bhattacharjee, T. Dey, A.K. Ghosh, M. Mandal, S.C. Kundu, Hydroxyapatite reinforced inherent RGD containing silk fibroin composite scaffolds: Promising platform for bone tissue engineering, Nanomed- Nanotechnol. 13 (2017) 1745–1759.